

# Arctic ozone depletion in 2019/20: Roles of chemistry, dynamics and the Montreal Protocol

Wuhu Feng<sup>1,2</sup>, Sandip S. Dhomse<sup>1,3</sup>, Carlo Arosio<sup>4</sup>, Mark Weber<sup>4</sup>, John P. Burrows<sup>4</sup>,  
Michelle L. Santee<sup>5</sup> and Martyn P. Chipperfield<sup>1,3</sup>

<sup>1</sup>School of Earth and Environment, University of Leeds, Leeds, UK.

<sup>2</sup>National Centre for Atmospheric Science, University of Leeds, Leeds UK.

<sup>3</sup>National Centre for Earth Observation, University of Leeds, UK.

<sup>4</sup>Institute of Environmental Physics, University of Bremen, Bremen, Germany

<sup>5</sup>Jet Propulsion Laboratory, California Institute of Technology, Pasadena, CA, USA.

Corresponding author: Wuhu Feng ([W.Feng@leeds.ac.uk](mailto:W.Feng@leeds.ac.uk)) and Martyn Chipperfield  
([M.Chipperfield@leeds.ac.uk](mailto:M.Chipperfield@leeds.ac.uk))

## Special GRL section: The Exceptional Arctic Polar Vortex in 2019/2020: Causes and Consequences

### Key Points:

- Large mean Arctic chemical ozone destruction (>63°N) in 2019/20 of 78 DU, similar to other extreme cold winters in the past two decades.
- Anomalously weak wintertime dynamical replenishment of only ~60 DU contributed strongly to the very low observed ozone column in March.
- Ozone recovery caused 20 DU less mean Arctic ozone loss in March 2020 than would have occurred with stratospheric halogens at 1995 levels.

## Abstract

We use a 3-D chemical transport model and satellite observations to investigate Arctic ozone depletion in winter/spring 2019/20 and compare with earlier years. Persistently low temperatures caused extensive chlorine activation through to March. March-mean polar-cap-mean modelled chemical column ozone loss reached 78 DU (local maximum loss of ~108 DU in the vortex), similar to that in 2011. However, weak dynamical replenishment of only 59 DU from December to March was key to producing very low (<220 DU) column ozone values. The only other winter to exhibit such weak transport in the past 20 years was 2010/11, so this process is fundamental to causing such low ozone values. A model simulation with peak observed stratospheric total chlorine and bromine loading (from the mid-1990s) shows that gradual recovery of the ozone layer over the past two decades ameliorated the polar cap ozone depletion in March 2020 by ~20 DU.

## Plain Language Summary

Ozone depletion in the polar stratosphere is caused by chlorine and bromine species which are activated by low temperatures. This chlorine and bromine is transported to the stratosphere following the surface emission of ozone-depleting substances (ODSs). While springtime ozone depletion in the Antarctic is almost always large, it is much more variable in the Arctic due to warmer temperatures and more disturbed stratospheric dynamics. Using a 3-D atmospheric chemical transport model and satellite observations, we show that the very low ozone columns observed in March 2020 were a consequence of large chemical destruction and weaker-than-normal replenishment by dynamics. These very low ozone levels are, by some measures, record values despite two decades of decreasing stratospheric chlorine and bromine through controls of the Montreal Protocol. Had the meteorology of 2019/20 occurred two decades ago the ozone loss would have been notably larger. The Arctic stratospheric dynamics for 2019/20 are extreme relative to the past two decades but fit a compact relationship that links column ozone variations over Arctic and Antarctic winters.

## 1 Introduction

Polar springtime ozone depletion is caused by catalytic cycles involving ClO and BrO radicals. Stratospheric chlorine is converted from reservoir forms (e.g. HCl and ClONO<sub>2</sub>) to active, ozone-destroying forms (ClO<sub>x</sub> = ClO + 2Cl<sub>2</sub>O<sub>2</sub>) by processing on the surfaces of polar stratospheric clouds (PSCs) (Peter 1997; Solomon 1999). As PSCs require low temperatures ( $\leq 195$  K) to form, there is large interannual variability in the extent of ozone depletion in the Arctic (e.g. Pitts et al., 2018).

Column ozone abundances in the Arctic are also strongly affected by interannual dynamical variability (e.g. Randel et al., 2002; Tegtmeier et al., 2008; Weber et al., 2011). Polar descent leads to an increase in winter/spring column ozone and this effect can outweigh the magnitude of chemical ozone depletion, and also exhibits large interannual variability.

Chlorine and bromine are delivered to the stratosphere through the transport of surface-emitted ozone-depleting substances (ODSs), such as chlorofluorocarbons (CFCs) and hydrochlorofluorocarbons (HCFCs). Due to action taken under the Montreal Protocol, the tropospheric loadings of chlorine and bromine peaked in 1993 and 1997, respectively (WMO 2018), with the polar stratospheric loadings peaking around 7 years later. The subsequent slow decrease in the total loading of these halogens has led to the detection of ozone recovery (or healing) in the upper stratosphere (e.g. Newchurch et al., 2003) and in the Antarctic springtime lower stratosphere (e.g. Solomon et al., 2016). Some recovery is also expected in Arctic ozone but the large observed interannual variability has so far precluded its detection (Chipperfield et al., 2017).

Arctic winter 2019/20 experienced a sustained period of low temperatures in the lower stratosphere and a stable vortex that persisted into late March (Lawrence et al., 2020). These conditions were conducive to an unprecedented extent of PSC area (DeLand et al., 2020), large levels of ozone depletion of up to 2.8 parts per million by volume (ppmv) (Manney et al., 2020) and subsequently small total column values (Lawrence et al., 2020; Wohltmann et al. 2020). This large depletion rivalled or even exceeded that observed in 2010/11, the previous Arctic winter with record ozone depletion (Manney et al., 2011).

In this paper, we use a detailed atmospheric 3-D chemical transport model (CTM), evaluated using satellite data, to investigate Arctic ozone depletion in winter/spring 2019/20. A multi-decadal model run is used to compare this winter with others over the past few decades, in particular years with large ozone depletion. We use the model to distinguish between the roles of chemistry and transport in causing the low ozone values. We also use the model to quantify the extent of the ozone recovery signal in the Arctic.

## 2 TOMCAT 3-D CTM

We have performed a series of experiments with the TOMCAT/SLIMCAT (hereafter TOMCAT) 3-D CTM (Chipperfield, 2006). The model contains a detailed description of stratospheric chemistry, including heterogeneous reactions on sulfate aerosols and PSCs. The model was forced using European Centre for Medium-Range Weather Forecasts (ECMWF) ERA5 winds and temperatures (Hersbach et al., 2020) and run with a resolution of  $2.8^\circ \times 2.8^\circ$  with 32 levels from the surface to ~60 km following Dhomse et al. (2019). The surface mixing ratios of long-lived source gases (e.g. CFCs, HCFCs, CH<sub>4</sub>, N<sub>2</sub>O) were taken from WMO (2018) scenario A1. The solar cycle was included using time-varying solar flux data (1995-2019) from

the Naval Research Laboratory (NRL) solar variability model, referred to as NRLSSI2 (update of Coddington et al., 2016; 2019). Stratospheric sulfate aerosol surface density (SAD) data for 1995-2016 were obtained from [ftp://iacftp.ethz.ch/pub\\_read/luo/CMIP6/](ftp://iacftp.ethz.ch/pub_read/luo/CMIP6/) (Arfeuille et al., 2013; Dhomse et al., 2015). As year-to-year solar flux variations (and their effects on ozone) are small (e.g. Dhomse et al., 2016), solar fluxes from December 2019 are used to extend the simulation until April 2020. Similarly, SAD values are not yet available for the whole period; thus for 2017-2020 the monthly mean SAD values were repeated from 2016. The model has a passive ozone tracer for diagnosing polar chemical ozone loss which is initialised from the chemical ozone tracer every December 1 and June 1 (e.g., Feng et al., 2007).

We performed a total of three multi-decadal model simulations. The control run (CNTL) was spun up from 1977 and integrated until April 2020 including all of the processes described above. Sensitivity run ODS95 was initialised from CNTL in 1995 and integrated until 2020 using constant surface mixing ratios of halogenated ODSs at 1995 levels. Sensitivity run WA (World Avoided) was initialised from CNTL in 1987 and integrated to 2020 using an ODS scenario which assumes no controls from the Montreal Protocol but rather a continuing 3%/year growth in emissions. This follows on from Chipperfield et al. (2015) who studied the Arctic winter 2010/11 with a similar simulation; results are discussed in the Supplementary Material.

### 3 Satellite Datasets

To compare to our CNTL model simulation, we use observations from the Ozone Monitoring Instrument (OMI) (McPeters et al., 2008) level 3 (OMTO3d) total column data. The OMTO3d is a daily gridded dataset, generated by gridding and merging only high-quality level 2 measurements (based on a Total Ozone Mapping Spectrometer (TOMS)-like algorithm) for a given day. Data is available from 1 October 2004 at  $0.25^\circ \times 0.25^\circ$  resolution and is obtained via [https://search.earthdata.nasa.gov/search?q=OMDOAO3e\\_003](https://search.earthdata.nasa.gov/search?q=OMDOAO3e_003).

We also use the GOME-SCIAMACHY-GOME-2 (GSG) merged dataset (1995–2020), constructed by merging total column ozone from Global Ozone Monitoring Experiment (GOME), the Scanning Imaging Absorption Spectrometer for Atmospheric Chartography (SCIAMACHY), and GOME-2A instruments retrieved with the WFDOAS algorithm (e.g. Weber et al., 2011, 2018). The SCIAMACHY and GOME-2A data were successively bias corrected during overlap periods to the starting record of GOME. GSG data can be obtained from <http://www.iup.uni-bremen.de/UVSAT/datasets/merged-wfdoas-total-ozone>.

For height-resolved comparisons we use Aura-Microwave Limb Sounder (MLS) v4 level-2 data (2004-2020) for  $O_3$ ,  $N_2O$ ,  $HCl$ ,  $ClO$  and  $HNO_3$ . MLS data can be obtained from [https://search.earthdata.nasa.gov/search?q=ML2O3\\_00](https://search.earthdata.nasa.gov/search?q=ML2O3_00). MLS equivalent latitude zonal monthly means are calculated by binning the profiles at model latitude intervals. Note that due to degradation of the MLS 190 GHz receiver, the  $N_2O$  v4 data shows a drift which becomes apparent in 2010 (N. Livesey, personal communication, 2020). For this reason we do not use recent  $N_2O$  data. Note that this degradation does not affect the other species used here.

## 4 Results

### 4.1 Polar Processing

**Figure 1a-d** shows the anomaly in the monthly mean Arctic mean ( $63^{\circ}\text{N}$ - $90^{\circ}\text{N}$ ) mixing ratios of  $\text{N}_2\text{O}$ ,  $\text{HNO}_3$ ,  $\text{HCl}$  and  $\text{ClO}$  at 480 K from MLS and model run CNTL (2004 – 2020). The equivalent direct comparisons of Arctic mean mixing ratios are given in supplementary **Figure S1**. Due to the degradation of the MLS  $\text{N}_2\text{O}$  observations we do not show its observed anomaly. The Arctic winter 2019/20 stands out as extreme in the record of many of these species (Manney et al., 2020). Modelled  $\text{N}_2\text{O}$ , which compares well with MLS observations early in the record (**Figure S1a**), indicates strong descent in spring 2020. The  $\text{HNO}_3$  observations tend to show large negative anomalies in cold Arctic winters such as 2011, 2016 and 2020, and positive anomalies in warm winters such as 2015. Prior to 2020 the model captures this behaviour well, including the extreme 2015 and 2016 cases. However, in 2020 the model overestimates the negative anomaly (i.e. the model overestimates denitrification) compared to MLS, for which the winter does not appear as extreme. Together  $\text{HCl}$  and  $\text{ClO}$  indicate the extent of PSC processing and chlorine activation which, for example, produces negative  $\text{HCl}$  anomalies and positive  $\text{ClO}$  anomalies in cold years (e.g. 2005, 2008, 2011, 2016). For these species 2020 stands out as significant in terms of chlorine activation; the activation began earlier and lasted longer in 2019/20 than in the previous record winter 2010/11 (see also Manney et al., 2020). The model captures these variations in chlorine species well.

### 4.2 Ozone

**Figure 1e** shows the evolution of the monthly mean Arctic mean ozone anomaly at 480 K from MLS observations and model run CNTL. The largest observed anomalies occur in the springtime and vary between years with strong negative values (e.g. 2011, 2016) and strong positive values (e.g. 2019). These variations are captured well by the model. Within this time series 2020 stands out in both the observations and model as having the largest negative anomaly of ~35-40%.

Arctic winter/spring ozone levels are maintained by a balance of dynamics and chemical depletion, with both processes making large and variable contributions to the column amount in any year. **Figure 2a** shows the mean March Arctic column ozone from OMI observations versus model run CNTL. The OMI observations clearly show 2020 (315 DU) and 2011 (329 DU) as the two years with extremely low column ozone with, by this metric, slightly lower values in 2020. The chemical ozone tracer from model run CNTL captures the overall variation, and the two extreme years, very well. Results from the model run can be used to separate the contributions of dynamics and transport. The modelled passive ozone shows values between 306 DU (2015) and 355 DU (2018) in December, with little interannual variability. Descent over winter typically increases passive ozone to 460 – 530 DU (increase of 122 – 220 DU) in March, with much larger variability. However, both 2011 and 2020 stand out as significant anomalies with March mean passive ozone columns of 396 DU (increase of 64 DU) and 376 DU (increase of 59 DU), respectively. This shows that a relatively small increase over the winter due to weak transport contributed significantly to the overall low ozone columns in these years (see also Wohltmann et al., 2020). The model further suggests that the contribution of transport would have led to slightly lower column ozone in early spring 2020 than in 2011.

The difference between modelled active and passive tracers quantifies the seasonal chemical ozone loss (lower panel of **Figure 2a**). This metric shows interannual variability of between ~40 DU (in warm winter 2018/19) and ~80 DU (in 2015/16). Note that this metric, over this wide geographical area which combines inside and outside vortex regions, smooths out the larger variations in chemical ozone loss which occur in the vortex core. Nevertheless, 2019/20 does stand out as a year with large chemical ozone loss (~78 DU), which is comparable that in the other cold winters of 2004/05, 2010/11 and 2015/16. However, the model results show that anomalously weak transport played a decisive role in causing the overall low column ozone in winter 2019/20.

#### 4.3 Impact of Ozone Recovery

Although the chemical ozone depletion in Arctic winter 2019/20 has been shown to be large (Manney et al., 2020; Lawrence et al., 2020; Wohltmann et al., 2020), it will have been ameliorated to some extent by recent decreases in stratospheric halogen levels due to the Montreal Protocol. The differences in column ozone between runs CNTL and ODS95, which uses constant tropospheric ODS values from 1995, quantify the increase in ozone due to decreasing (from their peak) stratospheric halogens, often taken as a measure of recovery (**Figure 2b**). The increasing impact of decreasing halogens with time, especially in the polar regions, can clearly be seen. Depletion in the Antarctic ozone hole in 2019 is ~30 DU less severe than it would have been under conditions of peak stratospheric halogen loading. For the Arctic the impact varies but the increasing influence of halogen recovery and the favourable conditions for ozone loss produce the largest effect in 2020. This increasing recovery signal for March is also seen in **Figure 2a**; reductions in stratospheric halogens have resulted in mean column ozone depletion being ~20 DU less severe than it would have been at peak loading.

The mean behaviour of ozone in the polar region masks the variations within the vortex and local extreme values. **Figure 3a** shows OMI column ozone on March 18, 2020. This is during the phase of active PSCs (DeLand et al., 2020) and ongoing ozone loss, but it corresponds to the day of the lowest ozone column in the OMI record of 208 DU. This is well below the threshold of 220 DU which is commonly used to denote the boundary of the Antarctic ozone hole. Simulation CNTL (**Figure 3b**) gives a good representation of the spatial distribution of column ozone but produces larger regions below the 220 DU contour. **Figure 3c** shows, however, that transport alone (between December and March) would have led to relatively low column values inside the vortex. These low columns are exacerbated by chemical depletion of up to 108 DU in the vortex (**Figure 3d**) to produce the modelled column in **Figure 3b**. **Figures 3e** and **f** show results from run ODS95. While the mean ozone recovery signal is ~20 DU for the wider Arctic area (**Figure 2**), the differences peak at ~35 DU in the core of the vortex. Supplementary **Figure S3** shows the equivalent plots for March 30, 2020, at the end of the ozone depletion phase.

Chipperfield et al. (2015) used the TOMCAT 3-D CTM to quantify the benefits already achieved by the Montreal Protocol at the time of the large observed Arctic ozone depletion in 2010/11. They assumed a continuing scenario of 3% annual growth in ODS emissions after 1987. It is unlikely that we would have reached 2020 without some controls on the use of ODSs given the environmental damage that would have become apparent. However, we can use the model to investigate the impact on ozone by extending a similar ‘world avoided’ experiment

(WA) until winter 2019/20. Supplementary **Figure S4** shows that with the assumed continued growth in stratospheric chlorine and bromine, Arctic ozone loss would by now have already become extremely severe with March vortex columns of less than 85 DU.

#### 4.4 Dynamical Influence on Polar Ozone

Planetary wave driving of the wintertime polar stratosphere is typically stronger and more variable in the Northern Hemisphere (NH) compared to the Southern Hemisphere (SH), leading to a warmer Arctic polar vortex and less chemical ozone depletion. In contrast, the Antarctic polar vortex is much less disturbed by wave forcing and temperatures are almost always low enough for extensive springtime chemical ozone depletion (Solomon et al., 2014; WMO 2018). Weber et al. (2011) summarised the interannual variability and interhemispheric differences by demonstrating a compact linear relationship between the mean winter eddy heat flux at 100 hPa and the spring-to-autumn high-latitude ozone ratio. This is shown in **Figure 4a**, which is an update of WMO (2018, Figure 4-12) with the addition of two Antarctic winters (2018 and 2019) and three Arctic winters (2017/18 – 2019/20) to the record starting in 1995/96. These additional winters confirm the established linear relationship with some notable new extremes falling between the usual clusters of NH and SH points. Antarctic winter 2019 compares with 2002 in being a year with strong wave driving and relatively small chemical ozone depletion (Kramarova et al., 2020), leading to a net positive change in ozone from autumn to spring. For the Arctic, winter 2019/20 is at the northern hemispheric extreme of weak wave driving and large ozone depletion and therefore appears similar to 2010/11.

The model control run CNTL captures the observed relationship (**Figure 4b**). This panel includes model years from the 1980s when stratospheric halogen loading was still increasing and the chemical ozone depletion was correspondingly less. Hence these points do not fall on the correlation lines for the three subsequent decades. It is interesting how little these lines differ, despite the decrease in stratospheric halogens since 1995. The impact of ozone recovery on this correlation is shown in **Figure 4c**, which shows results from the most recent decade for runs CNTL and ODS95. The larger halogen loading in run ODS95 does lead to lower ozone, especially in the Antarctic, but the effect on the slope is relatively small. As stratospheric halogens decay further, and recovery continues, chemical depletion will return to 1980s levels and the compact correlation can be expected to change significantly.

## 5 Discussion and Conclusions

We have shown that by many metrics the Arctic winter/spring 2019/20 exhibited extreme behaviour within the record of the past two decades. Our 3-D TOMCAT/SLIMCAT CTM captures well the observed persistent low temperatures and strong chlorine activation in the lower stratosphere and shows that the extremely low column ozone abundances arose through a combination of chemical loss and weak replenishment through transport. Despite the large chemical depletion, the model shows that recovery since the peak stratospheric halogen loading ameliorated the loss by ~20 DU. Without the Montreal Protocol at all, the ozone loss would have been extremely large. The unusual dynamics of Arctic winter 2019/20 fits well to the previously established correlation of spring/autumn ozone column and wintertime eddy heat flux for both polar regions.

Stratospheric chlorine and bromine loadings are decreasing and signs of ozone recovery have been detected. Nevertheless, winter 2019/20 has shown that the Arctic is still susceptible to very large (even record) ozone depletion under suitable meteorological conditions. Due to the Montreal Protocol, the potential for halogen-catalysed polar ozone depletion will gradually decrease. However, the potential for weak dynamical events to cause low column ozone will remain and so there is a need for continued monitoring and process understanding of this part of the atmosphere.

## Acknowledgments

This work was supported by the NERC SISLAC project (NE/R001782/1). We thank ECMWF for providing their analyses. The model simulations were performed on the national Archer and Leeds ARC HPC facilities. Work at the Jet Propulsion Laboratory, California Institute of Technology, was carried out under a contract with the National Aeronautics and Space Administration. The financial support of part of this work from the State of Bremen, DAAD grant (CA), and ESA SOLVE Living Planet Fellowship (CA) is gratefully acknowledged.

## Data Availability Statement

OMI data is available via [https://search.earthdata.nasa.gov/search?q=OMDOAO3e\\_003](https://search.earthdata.nasa.gov/search?q=OMDOAO3e_003). GSG data can be obtained from <http://www.iup.uni-bremen.de/UVSAT/datasets/merged-wfdoas-total-ozone>. MLS data can be obtained from [https://search.earthdata.nasa.gov/search?q=ML2O3\\_00](https://search.earthdata.nasa.gov/search?q=ML2O3_00). Stratospheric sulfate aerosol surface density (SAD) data for 1995-2016 were obtained from [ftp://iacftp.ethz.ch/pub\\_read/luo/CMIP6/](ftp://iacftp.ethz.ch/pub_read/luo/CMIP6/). NRLSSI2 data is accessible from [https://lasp.colorado.edu/lisird/data/nrl2\\_ssi\\_P1M/](https://lasp.colorado.edu/lisird/data/nrl2_ssi_P1M/). All data used in this paper, including the model results, are available from <http://doi.org/10.5281/zenodo.4294263>.

## References

- Arfeuille, F., Luo, B. P., Heckendorn, P., Weisenstein, D., Sheng, J. X., Rozanov, E., Schraner, M., Brönnimann, S., Thomason, L. W., & Peter, T. (2013). Modeling the stratospheric warming following the Mt. Pinatubo eruption: uncertainties in aerosol extinctions. *Atmos. Chem. Phys.*, *13*, 11221-11234, doi:10.5194/acp-13-11221-2013.
- Chipperfield, M. (2006). New version of the TOMCAT/SLIMCAT off-line chemical transport model: Intercomparison of stratospheric tracer experiments. *Q. J. Roy. Meteorol. Soc.*, *132*, 1179-1203.
- Chipperfield, M. P., Bekki, S., Dhomse, S., Harris, N. R. P., Hassler, B., Hossaini, R., Steinbrecht, W., Thiéblemont, R., & Weber, M. (2017). Detecting recovery of the stratospheric ozone layer. *Nature*, *549*, 211–218, doi:10.1038/nature23681.
- Chipperfield, M. P., Dhomse, S. S., Feng, W., McKenzie, R. L., Velders G., & Pyle J. A. (2015). Quantifying the ozone and UV benefits already achieved by the Montreal Protocol. *Nature Communications*, *6*, 7233, doi:10.1038/ncomms8233.



- Chipperfield, M. P., Dhomse, S., Hossaini, R., Feng, W., Santee, M. L., Weber, M., Burrows, J. P., Wild, J. D., Loyola, D., & Coldewey-Egbers, M. (2018). On the cause of recent variations in lower stratospheric ozone. *Geophys. Res. Lett.*, *45*, 5718-5726, doi:10.1029/2018GL078071.
- Coddington, O., Lean, J., Pilewskie, P., Snow, M. & Lindholm, D. (2016). A solar irradiance climate data record. *Bull. Amer. Meteor. Soc.*, doi:10.1175/BAMS-D-14-00265.1.
- Coddington, O., Lean, J., Pilewskie, P., Snow, M., Richard, E., Kopp, G., et al. (2019). Solar Irradiance variability: comparisons of models and measurements. *Earth and Space Science*, *6*, 2525– 2555, doi:10.1029/2019EA000693.
- DeLand, M. T., Bhartia, P. K., Kramarova, N., & Chen, Z. (2020). OMPS LP Observations of PSC variability during the NH 2019-2020 season. *Geophys. Res. Lett.*, e2020GL090216.
- Dhomse, S., Chipperfield, M. P., Feng, W., Hossaini, R., Mann, G. W. & Santee, M. L. (2015). Revisiting the hemispheric asymmetry in mid-latitude ozone changes following the Mount Pinatubo eruption: A 3-D model study. *Geophys. Res. Lett.*, *42*, 3038-3047, doi:10.1002/2015GL063052.
- Dhomse, S., Chipperfield, M. P., Damadeo, R. P., Zawodny, J. M., Ball, W. T., Feng, W., Hossaini, R., Mann, G. W., & Haigh, J. D. (2016). On the ambiguous nature of the 11-year solar cycle signal in upper stratospheric ozone. *Geophys. Res. Lett.*, *43*, 7241-7249, doi:10.1002/2015GL069958.
- Dhomse, S. S., Feng, W., Montzka, S. A. et al. (2019). Delay in recovery of the Antarctic ozone hole from unexpected CFC-11 emissions. *Nature Communications*, *10*, 5781, doi:10.1038/s41467-019-13717-x.
- Feng, W., Chipperfield, M. P., Davies, S., von der Gathen, P., Kyrö, E., Volk, C. M., Ulanovsky, A., and Belyaev, G. (2007). Large chemical ozone loss in 2004/2005 Arctic winter/spring. *Geophys. Res. Lett.*, *34*, L09803, doi:10.1029/2006GL029098.
- Hersbach, H., Bell, B., Berrisford, P., et al. (2020). The ERA5 global reanalysis. *Q. J. Roy. Meteorol. Soc.*, *146*, 1999–2049, doi:10.1002/qj.3803.
- Kramarova, N., Newman, P. A., Nash, E. R., Strahan, S. E., Long, C. S., Johnson, B., Pitts, M., Santee, M. L., Petropavlovskikh, I., Coy, L., & de Laat, J. (2020). 2019 Antarctic ozone hole [in “State of the Climate in 2019”]. *Bull. Amer. Meteorol. Soc.*, *101*, S310-S312, doi:10.1175/2020BAMSStateoftheClimate.1.
- Langematz, U., Tully, M. (Lead Authors), et al. (2018). Chapter 4 in Scientific Assessment of Ozone Depletion: 2018 Global Ozone Research and Monitoring Project Report No. 58, 588 pp, World Meteorological Organization, Geneva, Switzerland.
- Lawrence, Z. D., Perlwitz, J., Butler, A. H., Manney, G. L., Newman, P. A., Lee, S. H., & Nash, E. R. (2020). The remarkably strong Arctic stratospheric polar vortex of winter 2020: Links to record-breaking Arctic Oscillation and ozone loss. *J. Geophys. Res.*, *125*, e2020JD033271, doi:10.1029/2020JD033271.
- Manney, G. L., Santee, M. L., Rex, M., Livesey, N. J., Pitts, M. C., Veefkind, P., et al. (2011). Unprecedented Arctic ozone loss in 2011. *Nature*, *478*, 469-475, doi:10.1038/nature10556.
- Manney, G. L., Livesey, N. J., Santee, M. L., Froidevaux, L., Lambert, A., & Lawrence, Z. D., et al. (2020). Record-low Arctic stratospheric ozone in 2020: MLS observations of chemical

- processes and comparisons with previous extreme winters. *Geophys. Res. Lett.*, *47*, e2020GL089063. doi:10.1029/2020GL089063.
- McPeters, R. D., Kroon, M., Labow, G., Brinksma, E. J., Balis, D., Petropavlovskikh, I., Veefkind, J. P., Bhartia, P. K., & Levelt, P. F. (2008). Validation of the Aura Ozone Monitoring Instrument total column ozone product. *J. Geophys. Res.*, *113*, D15S14, doi:10.1029/2007JD008802.
- Newchurch, M. J., Yang, E.-S., Cunnold, D. M., Reinsel, G. C., Zawodny, J. M. & Russell, J. M. (2003). Evidence for slowdown in stratospheric ozone loss: First stage of ozone recovery. *J. Geophys. Res.*, *108*, 4507, doi:10.1029/2003JD003471.
- Peter, T. (1997). Microphysics and heterogeneous chemistry of polar stratospheric clouds. *Annual Review of Physical Chemistry*, *48*, 785-822, doi:10.1146/annurev.physchem.48.1.785.
- Pitts, M. C., Poole, L. R., & Gonzalez, R. (2018). Polar stratospheric cloud climatology based on CALIPSO spaceborne lidar measurements from 2006 to 2017. *Atmos. Chem. Phys.*, *18*, 10881-10913, doi:10.5194/acp-18-10881-2018.
- Solomon, S. (1999). Stratospheric ozone depletion: A review of concepts and history. *Rev. Geophys.*, *37*, 275-316, doi:10.1029/1999RG900008.
- Randel, W. J., Wu, F., & Stolarski, R. (2002). Changes in column ozone correlated with the stratospheric EP flux. *J. Meteorol. Soc. Japan*, *80*, 849-862, doi:10.2151/jmsj.80.849.
- Solomon, S., Haskins, J., Ivy, D. J., & Min, F. (2014). Fundamental differences between Arctic and Antarctic ozone depletion. *Proc. Natl. Acad. Sci. U.S.A.*, *111*, 6220-6225, doi:10.1073/pnas.1319307111.
- Solomon, S., Ivy, D. J., Kinnison, D., Mills, M. J., Neely, R. R., & Schmidt, A. (2016). Emergence of healing in the Antarctic ozone layer. *Science*, *353*, 269-274, doi:10.1126/science.aae0061.
- Tegtmeier, S., Rex, M., Wohltmann, I. and Krüger, K. (2008). Relative importance of dynamical and chemical contributions to Arctic wintertime ozone. *Geophys. Res. Lett.*, *35*, L17801, doi:10.1029/2008GL034250.
- Weber, M., Dikty, S., Burrows, J. P., Garny, H., Dameris, M., Kubin, A., Abalichin, J., & Langematz, U. (2011). The Brewer-Dobson circulation and total ozone from seasonal to decadal time scales. *Atmos. Chem. Phys.*, *11*, 11221-11235, doi:10.5194/acp-11-11221-2011.
- Weber, M., Coldewey-Egbers, M., Fioletov, V. E., Frith, S. M., Wild, J. D., Burrows, J. P., Long, C. S., & Loyola, D. (2018). Total ozone trends from 1979 to 2016 derived from five merged observational datasets – the emergence into ozone recovery. *Atmos. Chem. Phys.*, *18*, 2097-2117, doi:10.5194/acp-18-2097-2018.
- Wohltmann, I., von der Gathen, P., Lehmann, R., Maturilli, M., Deckelmann, H., Manney, G. L., et al. (2020). Near-complete local reduction of Arctic stratospheric ozone by severe chemical loss in spring 2020. *Geophys. Res. Lett.*, *47*, e2020GL089547, doi:10.1029/2020GL089547.
- WMO (2018). World Meteorological Organization (WMO) / United Nations Environment Programme (UNEP), Scientific Assessment of Ozone Depletion: 2018 Global Ozone Research and Monitoring Project Report No 58, 588 pp, World Meteorological Organization, Geneva, Switzerland.

388

389 **Figure 1.** Time series of percentage anomaly in monthly values of (a)  $\text{N}_2\text{O}$ , (b)  $\text{HNO}_3$ , (c)  $\text{HCl}$ ,  
 390 (d)  $\text{ClO}$  and (e)  $\text{O}_3$  from 2004–2020 from MLS observations and model runs CNTL and ODS95  
 391 averaged from  $63^\circ\text{N}$ – $90^\circ\text{N}$  equivalent latitude at 480 K (approx. 18 km). The model was sampled  
 392 daily at the same local time as the MLS observations. There is no MLS data in panel (a). Results  
 393 from simulation ODS95 are not included in panels (a) and (b) as they are indistinguishable from  
 394 simulation CNTL.

395 **Figure 2.** (a) Arctic ( $63^\circ\text{N}$ – $90^\circ\text{N}$ , geographical latitude) monthly mean column ozone (DU) from  
 396 2004 to 2020. The upper panel shows March OMI observations and model simulations CNTL  
 397 and ODS95. The dashed lines show the passive ozone from CNTL for March (blue) and the  
 398 previous December (green). The lower panel shows the difference in mean March ozone between  
 399 runs CNTL and ODS95 (green) and the differences in the March passive – active ozone for runs  
 400 CNTL (blue) and ODS95 (red). The solid blue line is the difference in the mean passive ozone  
 401 from March – December. (b) Global distribution of differences in column ozone between model  
 402 run CNTL and ODS95 (DU).

403  
 404 **Figure 3.** Total Column ozone (TOZ, unit: DU) on March 18<sup>th</sup> 2020 (a) observed by OMI, (b)  
 405 from model run CNTL, (c) passive ozone from CNTL, and (e) from model run ODS95. (d)  
 406 Chemical ozone loss (DU) from run CNTL (active – passive). (f) Difference in column ozone  
 407 (DU) between runs ODS95 and CNTL. In panels (a), (b) and (e) the 220 DU contour is indicated  
 408 in white. In panels (d) and (f) the -100 and -20 DU contours, respectively, are dotted white.

409  
 410 **Figure 4.** Spring-to-autumn ratio of observed polar cap total ozone ( $>50^\circ$ ) as a function of the  
 411 absolute extratropical winter mean eddy heat flux (September to March and March to September  
 412 in the respective hemispheres) derived from (a) GSG ozone and ECMWF ERA5 meteorological  
 413 data (1995–2020) separately in the respective hemisphere, (b) model run CNTL (1980–2020) for  
 414 four decades (see colour code in legend) and (c) model runs CNTL and ODS95 (2011–2020, see  
 415 legend). Data from the Southern Hemisphere are shown as triangles (September over March  
 416 ozone ratios) and from the Northern Hemisphere as solid circles (March over September ratios).  
 417 Panel (a) is updated from Weber et al. (2011) and WMO (2018), and the points are coloured  
 418 according to the decade as in panel (b). Only selected years are labelled in panels (a) and (b).

419  
 420

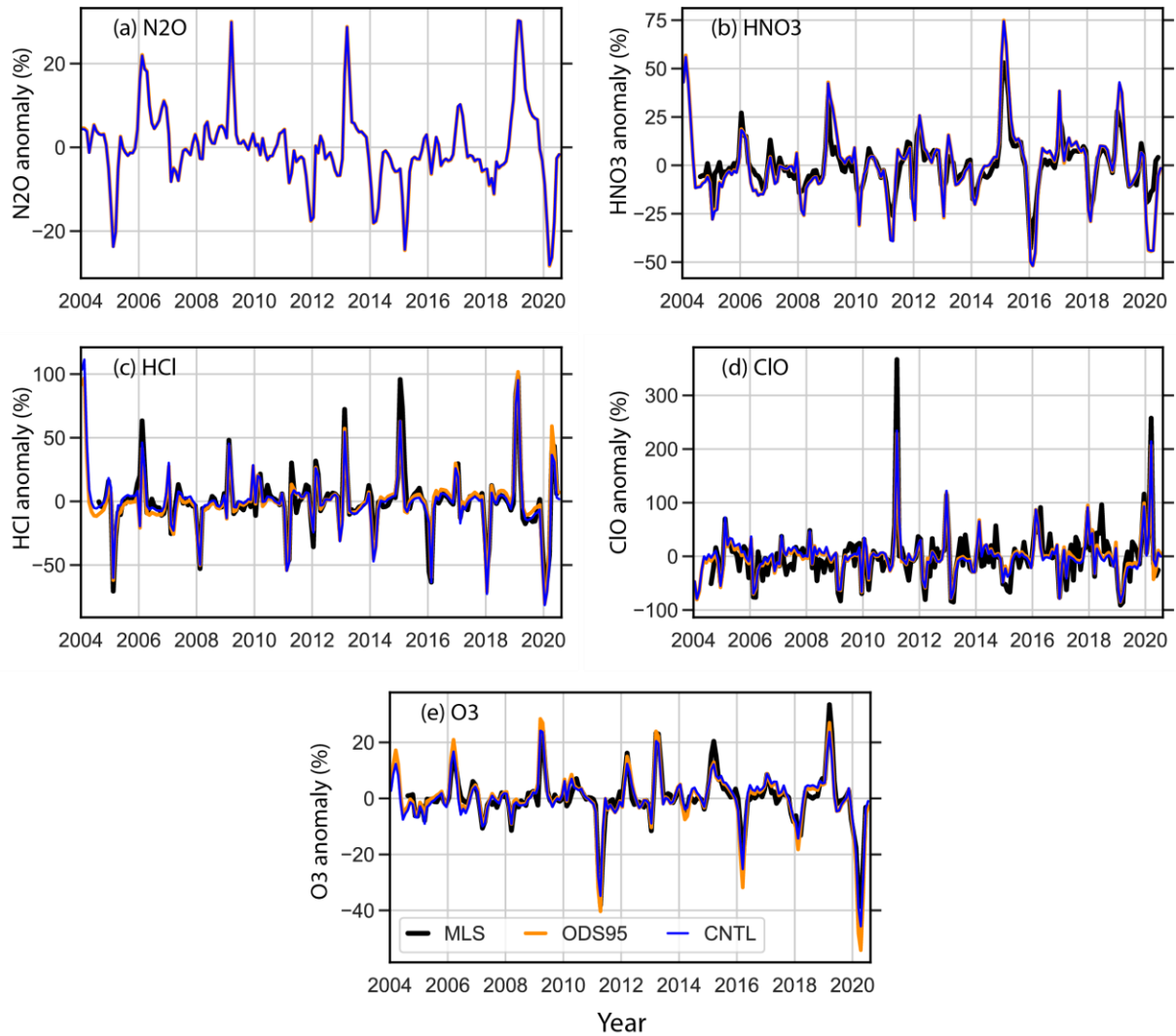
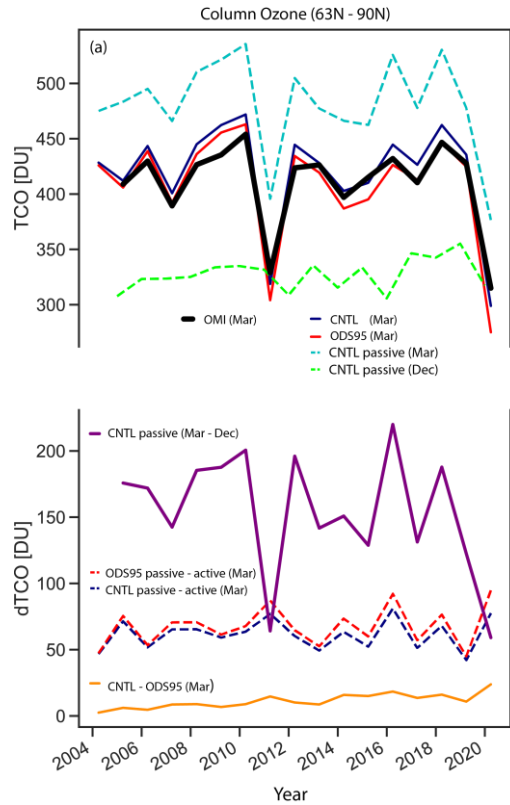
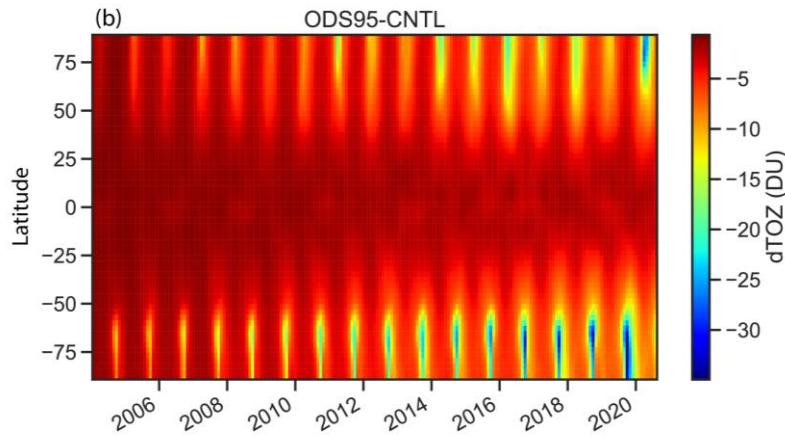


**Figure 1.** Time series of percentage anomaly in monthly values of (a)  $\text{N}_2\text{O}$ , (b)  $\text{HNO}_3$ , (c)  $\text{HCl}$ , (d)  $\text{ClO}$  and (e)  $\text{O}_3$  from 2004-2020 from MLS observations and model runs CNTL and ODS95 averaged from  $63^\circ\text{N}$ - $90^\circ\text{N}$  equivalent latitude at 480 K (approx. 18 km). The model was sampled daily at the same local time as the MLS observations. There is no MLS data in panel (a). Results from simulation ODS95 are not included in panels (a) and (b) as they are indistinguishable from simulation CNTL.

431



432



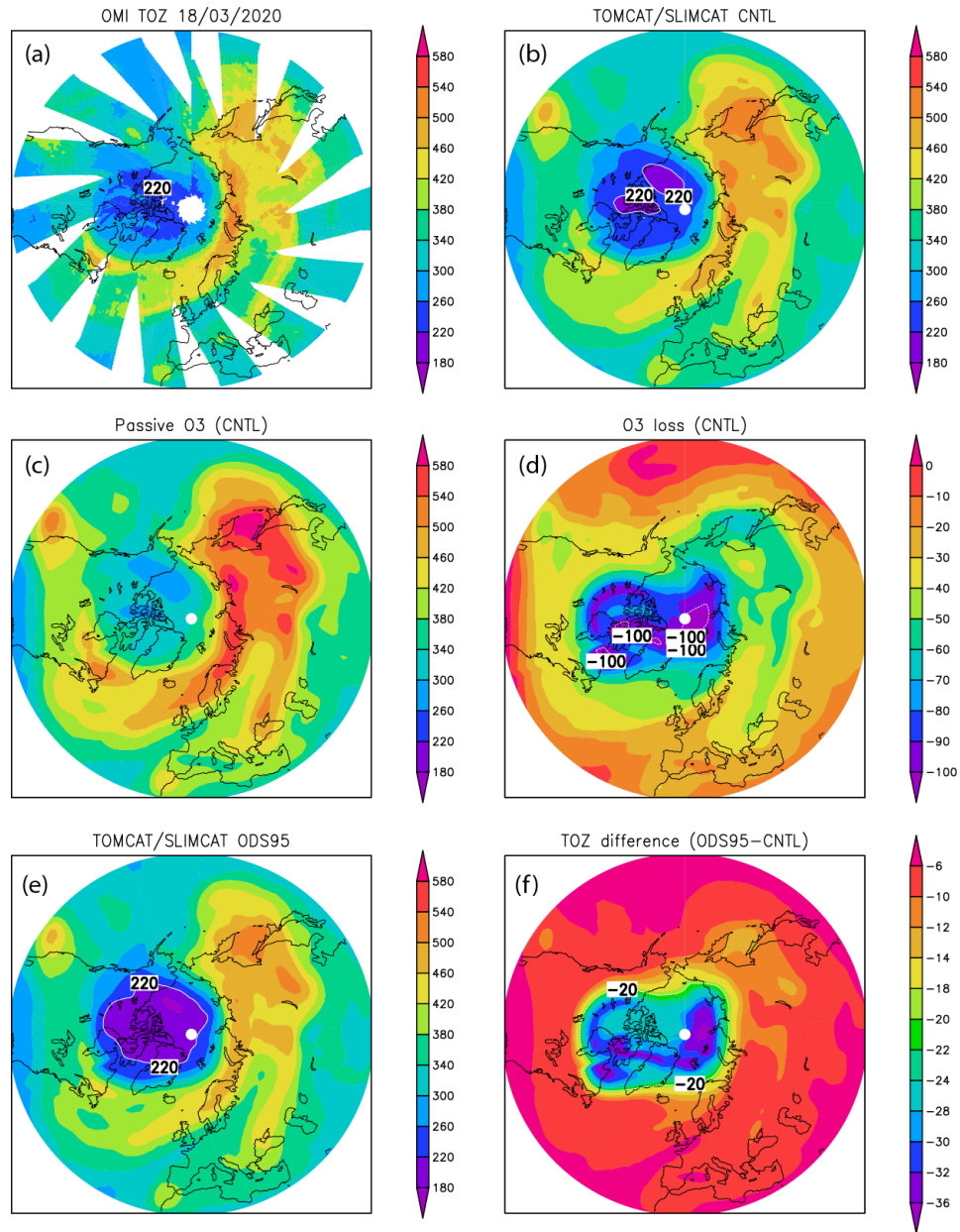
433

434

435 **Figure 2.** (a) Arctic (63°N-90°N, geographical latitude) monthly mean column ozone (DU) from  
 436 2004 to 2020. The upper panel shows March OMI observations and model simulations CNTL  
 437 and ODS95. The dashed lines show the passive ozone from CNTL for March (blue) and the  
 438 previous December (green). The lower panel shows the difference in mean March ozone between  
 439 runs CNTL and ODS95 (green) and the differences in the March passive – active ozone for runs  
 440 CNTL (blue) and ODS95 (red). The solid blue line is the difference in the mean passive ozone  
 441 from March – December. (b) Global distribution of differences in column ozone between model  
 442 run CNTL and ODS95 (DU).

443

444



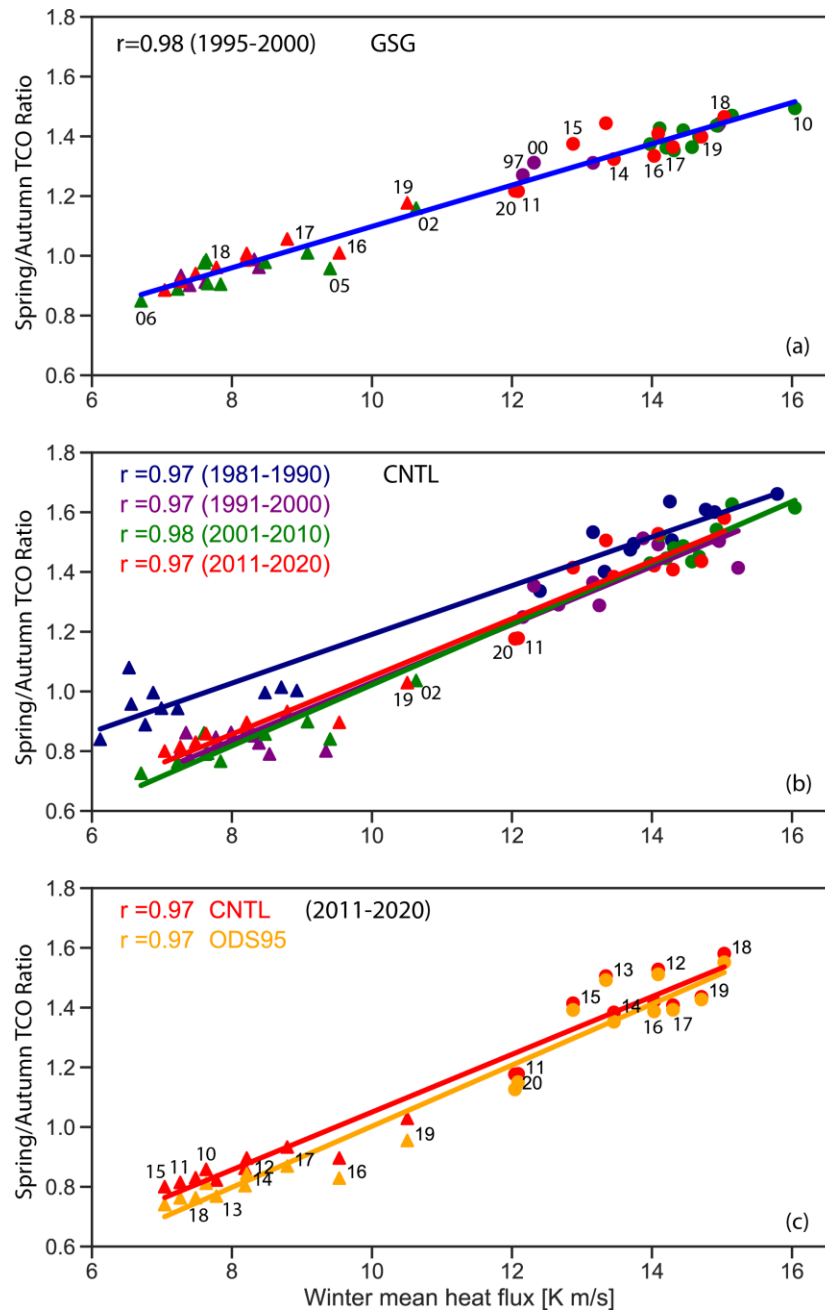
445

446

447 **Figure 3.** Total Column ozone (TOZ, unit: DU) on March 18<sup>th</sup> 2020 (a) observed by OMI, (b)  
 448 from model run CNTL, (c) passive ozone from CNTL, and (e) from model run ODS95. (d)  
 449 Chemical ozone loss (DU) from run CNTL (active – passive). (f) Difference in column ozone  
 450 (DU) between runs ODS95 and CNTL. In panels (a), (b) and (e) the 220 DU contour is indicated  
 451 in white. In panels (d) and (f) the -100 and -20 DU contours, respectively, are dotted white.

452

453



454

455

456 **Figure 4.** Spring-to-autumn ratio of observed polar cap total ozone ( $>50^\circ$ ) as a function of the  
 457 absolute extratropical winter mean eddy heat flux (September to March and March to September  
 458 in the respective hemispheres) derived from (a) GSG ozone and ECMWF ERA5 meteorological  
 459 data (1995-2020) separately in the respective hemisphere, (b) model run CNTL (1980-2020) for  
 460 four decades (see colour code in legend) and (c) model runs CNTL and ODS95 (2011-2020, see  
 461 legend). Data from the Southern Hemisphere are shown as triangles (September over March  
 462 ozone ratios) and from the Northern Hemisphere as solid circles (March over September ratios).  
 463 Panel (a) is updated from Weber et al. (2011) and WMO (2018), and the points are coloured  
 464 according to the decade as in panel (b). Only selected years are labelled in panels (a) and (b).